European Journal of Soil Science

*European Journal of Soil Science*, October 2013, **64**, 716–727 doi: 10.1111/ejss.12067

# Integrating multi-receiver electromagnetic induction measurements into the interpretation of the soil landscape around the school of gladiators at Carnuntum

T. Saey[a], M. Van Meirvenne[a], P. De Smedt[a], W. Neubauer[b], I. Trinks[b], G. Verhoeven[b] & S. Seren[c]

[a]*Research Group Soil Spatial Inventory Techniques, Engineering, Ghent University, B-9000 Gent, Belgium,* [b]*Ludwig Boltzmann Institute for Archaeological Prospection and Virtual Archaeology, A-1190 Vienna, Austria, and* [c]*Department of Geophysics, Central Institute for Meteorology and Geodynamics, A-1190, Vienna, Austria*

## Summary

Recently, the unique foundations of a school of gladiators were discovered in the Roman town of Carnuntum (40 km southeast of Vienna, Austria) by applying a combination of non-invasive archaeological prospection techniques such as magnetometry, ground penetrating radar, aerial photography, airborne laser scanning and airborne imaging spectroscopy. Although the well-preserved remains of the building complex were revealed down to a depth of 1.8 m by high-resolution near-surface geophysics, some questions about the surrounding soil landscape remained unanswered. Therefore, a proximal soil sensing procedure based on a survey with a multi-receiver electromagnetic induction (EMI) instrument was conducted to interpret the surroundings of the school, covering an area of 5.6 ha. We investigated the usefulness of integrating the complementary apparent electrical conductivity (ECa) and apparent magnetic susceptibility (MSa) measurements for the mapping and investigation of this soil landscape. The multiple ECa measurements allowed the identification of zones with low-conductive gravel outcrops, and zones where silty-clayey soils were deposited on top of the underlying gravel. An EC-depth slicing procedure enhanced the contrast between small soil features, such as frost-wedge pseudomorphs and drainage gullies, and their background, and provided indications about the depth extent of these features. The MS-depth slices showed the foundations of the school of gladiators, an aqueduct and grave monuments. After combining these results with the topography, an integrated visualization of the school in its soil landscape was obtained. This study demonstrated the potential of multi-receiver EMI soil surveys to map and interpret the soil landscape and to discern small natural as well as archaeological features.

## Introduction

Over the past decade the use of geophysical prospection methods for archaeological applications has increased substantially (Van Dam, 2012) and magnetometry, Earth resistance measurements (ERTs) and ground penetrating radar (GPR) are frequently used (Gaffney & Gater, 2003). Much less common is the application of low frequency electromagnetic induction (EMI) methods. However, the latter methods have been well used for proximal soil sensing (Viscarra Rossel *et al.*, 2011) and precision agriculture because measurements of the apparent electrical conductivity (ECa) and its reciprocal, apparent electrical resistivity ($\rho_a$), allow the detailed characterization of the variability of soil properties such as texture, organic matter and moisture (McBratney *et al.*, 2005; Heil & Schmidhalter, 2012). While EMI methods have greater signal-to-noise ratio in conductive soils, the ERT method is more suitable for investigating resistive materials (Clark, 1997). Initially, most of the proximal soil sensors focused on lateral variations of ECa and $\rho_a$; however, vertical variations are also informative. Therefore, multi-receiver ERT (Lück & Ruehlmann, 2013) and EMI systems (Saey *et al.*, 2009a) have been developed.

Electromagnetic induction sensors also allow us to obtain simultaneous measurements of the soil apparent magnetic susceptibility (MSa). Although similar to magnetometry, MSa provides additional information and the difference lies in the source of the induced magnetic field. Instruments that use EMI actively create an electromagnetic field directly above the ground and measure the response from nearby material. In contrast, magnetometry is

Correspondence: T. Saey. E-mail: Timothy.Saey@UGent.be

Received 8 November 2012; revised version accepted 9 May 2013

a passive technique, which relies on the Earth's magnetic field as the primary inducing field (Simpson *et al.*, 2009).

The depth sensitivity profile of an EMI sensor depends on the distance between the transmitter and receiver coil, the orientation of the coils and the applied frequency (Thiesson *et al.*, 2009). To increase their applicability, some EMI instruments allow the modulation of the transmitting frequency, while others have multiple receiver coils that allow the discrimination of vertical contrasts in ECa and MSa (Monteiro Santos *et al.*, 2010). When such information is available over a wider area, it is possible to compose detailed, three-dimensional reconstructions of the soil variation (Saey *et al.*, 2011a). These reconstructions are complementary to the information gathered with conventional methods, guiding the understanding of the buried archaeological structures (De Clercq *et al.*, 2012).

Recently, the Ludwig Boltzmann Institute for Archaeological Prospection and Virtual Archaeology (LBI ArchPro), currently engaged in the archaeological prospection of the archaeological landscape Carnuntum (Neubauer *et al.*, 2012; Trinks *et al.*, 2012), announced the discovery of the buried remains of the school of gladiators (*ludus gladiatorius*) next to the excavated amphitheatre of the Roman civil town of Carnuntum in Austria (Humer, 2012). This was achieved by combining aerial archaeology, airborne imaging spectroscopy and airborne laser scanning with high-resolution magnetometry and multichannel GPR measurements at close range or in contact with the soil (Neubauer *et al.*, 2012).

However, these methods, focussing on the archaeological remains, only provided limited information about the variability in composition of the surrounding soil. This variability could offer insights into the interactions between humans and the surrounding soil landscape or into the way that their behaviours respond to different soil landscape structures.

The aim of this paper is to evaluate the usefulness of integrating multiple ECa and MSa signals from a multi-receiver EMI instrument to characterize the soil landscape around the archaeological site and, at the same time, the anthropogenic features of the soil. Therefore, we focus on (i) combining the multiple ECa measurements, (ii) integrating the multiple MSa measurements and (iii) merging the complementary ECa and MSa calculations at simultaneous depths to allow an enhanced interpretation of the soil landscape around the school of gladiators.

## Materials and methods

### *The Roman city of Carnuntum and the case study area*

The Roman city of Carnuntum was located some 40 km southeast of Vienna on the southern bank of the river Danube (Figure 1). As the capital of the Roman province Pannonia, between the second and fourth century AD, it was home to an estimated population of at least 50 000 inhabitants. Outside the gates of the city one of the largest amphitheatres of the Roman Empire was found. After the invasion of Germanic tribes in the fourth century AD, the city was completely destroyed and today only the remains of a triumphal arch survive above ground (Neubauer *et al.*, 2002). At the beginning of the 20th century AD the amphitheatre was discovered and its foundations were excavated between 1923 and 1930. Today, the buried remains of the Roman town and its surroundings are protected and the current permissions do not include destructive prospection methods. Our study site comprises a 5.6-ha arable field with central (WGS 84) coordinates 48°06′38″N, 16°50′58″E, containing the gladiatorial school and bordering the excavated amphitheatre (Figure 1).

The survey area is located on slightly undulating, fluvial and gravel-rich terraces of the nearby river Danube. Near the end of the Weichselian glacial period the area was covered with aeolian loess deposits with a variable but generally limited thickness. The soil in the area is classified as a Calcic Chernozem (Neubauer *et al.*, 2002; IUSS Working Group WRB, 2006). The study area slopes to the northwest with a range in elevation of 12.9 m (Figure 8a). No visible traces of soil erosion were observed at the soil surface of the site during our fieldwork.

### *Multi-receiver EMI soil sensor*

In its simplest configuration, an EMI soil sensor consists of two coils separated by a given fixed distance. A primary magnetic field ($H_p$) is created by an alternating current in the transmitting coil. This field exposed to the soil causes electrical currents (eddy currents), which induce a secondary magnetic field ($H_i$). Primary and secondary fields induce an alternating current in the receiving coil (McNeill, 1980). The real component of the total field (the amplitude at the quadrature-phase) is related to the ECa. The imaginary component (the amplitude of the in-phase) corresponds to the MSa, which is generally accepted as a measure of the magnetic susceptibility.

We used an EMI sensor (Dualem Inc., Milton, Canada) that consists of one transmitter coil and four receiver coils located at 1, 1.1, 2 and 2.1 m distance from the transmitter coil (Saey *et al.*, 2009a). The 1 and 2 m transmitter-receiver coil pairs form a horizontal coplanar dipole mode (HCP-1 and HCP-2), while the 1.1 and 2.1 m pairs form a perpendicular dipole mode (PRP-1 and PRP-2). Both transmitter-receiver spacing and orientation determine the depth and weighting response pattern of the signal. McNeill (1980) defined the depth response functions of EMI instruments in homogeneous soils by asymptotic approximations of the Maxwell equations (Maxwell, 1865; Fleisch, 2008). Hendrickx *et al.* (2002) proved that these approximations were valid for heterogeneous soils. The cumulative ECa response (expressed as % of the measured signal, relative to 1) from a soil volume above a depth $z$ (in m) was given by McNeill (1980) for the HCP dipole mode ($R_{\mathrm{HCP,ECa}}(z)$), and by Wait (1962) for the PRP dipole mode ($R_{\mathrm{PRP,ECa}}(z)$):

$$R_{\mathrm{HCP},s}(z) = 1 - \left(4 \cdot \frac{z^2}{s^2} + 1\right)^{-0.5}, \quad (1)$$

$$R_{\mathrm{PRP},s}(z) = 2\frac{z^2}{s^2}\left(4\frac{z^2}{s^2} + 1\right)^{-0.5}, \quad (2)$$

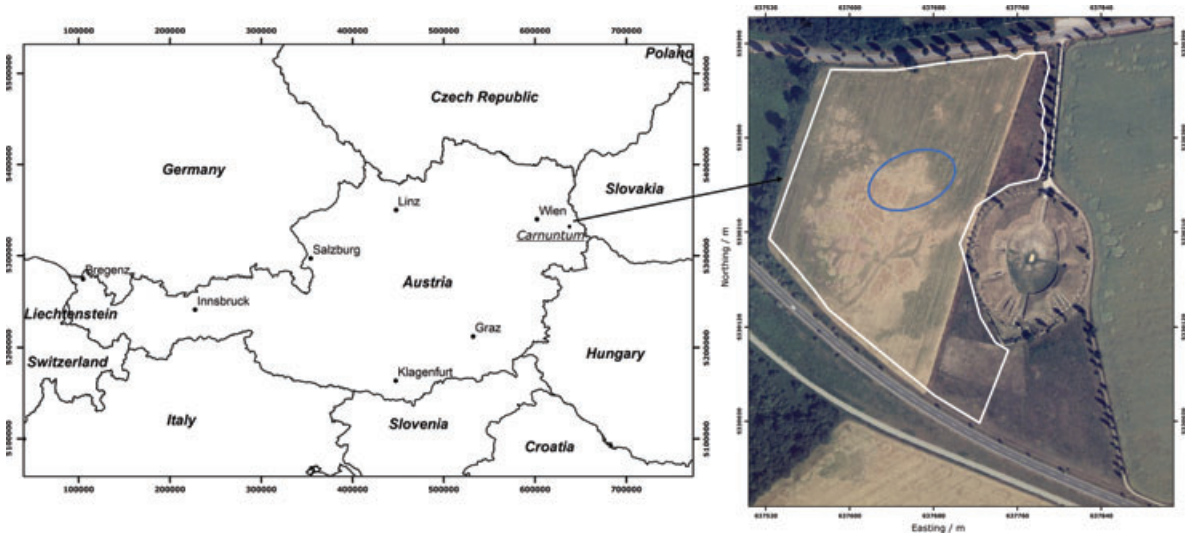


**Figure 1** Location of the study site in Austria and aerial photograph with indication of the site and the approximate position of the school of gladiators (oval).

with $s$ being the transmitter-receiver spacing. These cumulative response functions allow for the determination of the depth of exploration (DOE), conventionally defined as the depth above which 70% of the cumulative response is obtained from the soil volume. Obviously, this DOE differs for the different coil configurations: 0.5, 1.0, 1.5 and 3.2 m for the ECa of the PRP-1, PRP-2, HCP-1 and HCP-2 coil configurations, respectively (Figure 2). However, it must be noted that the ECa measurements can reflect the influence of deeper conductive material as well, because 30% of the response originates from soil material below the DOE.

Apparent magnetic susceptibility measurements in the PRP coil configurations are generally noisy because of instrumental instability and less useful than both measurements in HCP mode. However, it is possible to rotate the instrument by 90°, creating two vertical coplanar dipole coil configurations (VCP), with the receiver coils at 1 and 2 m distance from the transmitting coil. In such a position, the two PRP orientations correspond to a null-orientation, which is not responsive to a layered earth and therefore not operational (Frischknecht *et al.*, 1991). The cumulative depth responses for the MSa of the HCP and VCP dipole modes ($R_{\mathrm{HCP,MSa}}(z)$ and $R_{\mathrm{VCP,MSa}}(z)$) are given by McNeill (1980) (Figure 2):

$$R_{\mathrm{HCP},s}(z) = \frac{1 - 8\cdot\frac{z^2}{s^2}}{\left(4\cdot\frac{z^2}{s^2}+1\right)^{\frac{5}{2}}}, \tag{3}$$

$$R_{\mathrm{VCP},s}(z) = \frac{1}{\left(4\cdot\frac{z^2}{s^2}+1\right)^{\frac{3}{2}}}. \tag{4}$$

Thiesson *et al.* (2011) pointed out that the MSa measurements with an HCP coil orientation exhibit a change in the sign, which renders susceptibility measurements with this coil orientation difficult to interpret in relation to its depth. Nevertheless, the first 70% of the cumulative response of MSa with the HCP-1 configuration is obtained at a depth of 0.25 m, so for the HCP-2 configuration this becomes 0.5 m (Figure 2). The VCP orientation does not have such a change in sign and is therefore more straightforward to interpret. Seventy per cent of the cumulative response of the MSa measured with the VCP-1 configuration is obtained within the top 0.6 m, and for the VCP-2 configuration this becomes 1.2 m.

### *Depth-slicing*

The modelled electrical conductivity ($\mathrm{EC}^*$) or magnetic susceptibility ($\mathrm{MS}^*$) of a particular depth interval or slice can be deduced from the measured ECa or MSa values employing the depth sensitivity functions, Equations (1) and (2) or (3) and (4), respectively (Saey *et al.*, 2012). By establishing a set of four equations, the $\mathrm{EC}^*$ or $\mathrm{MS}^*$ (they are no longer 'apparent') of three layers with predefined depth boundaries can be estimated, given the height of the EMI sensor above the soil surface ($z_s$):

$$\begin{aligned}\mathrm{ECa}_{\mathrm{HCP},s} = &\left[R_{\mathrm{HCP},s}(z_1) - R_{\mathrm{HCP},s}(z_s)\right]\mathrm{EC}_1^* \\ &+ \left[R_{\mathrm{HCP},s}(z_2) - R_{\mathrm{HCP},s}(z_1)\right]\mathrm{EC}_2^* \\ &+ \left[1 - R_{\mathrm{HCP},s}(z_2)\right]\mathrm{EC}_3^*,\end{aligned} \tag{5}$$

$$\begin{aligned}\mathrm{ECa}_{\mathrm{PRP},s} = &\left[R_{\mathrm{PRP},s}(z_1) - R_{\mathrm{PRP},s}(z_s)\right]\mathrm{EC}_1^* \\ &+ \left[R_{\mathrm{PRP},s}(z_2) - R_{\mathrm{PRP},s}(z_1)\right]\mathrm{EC}_2^* \\ &+ \left[1 - R_{\mathrm{PRP},s}(z_2)\right]\mathrm{EC}_3^*,\end{aligned} \tag{6}$$

with $R_{\mathrm{HCP},s}(z)$ and $R_{\mathrm{PRP},s}(z)$ the cumulative ECa responses above depth $z$ for the HCP and PRP mode, respectively, and $s$ the

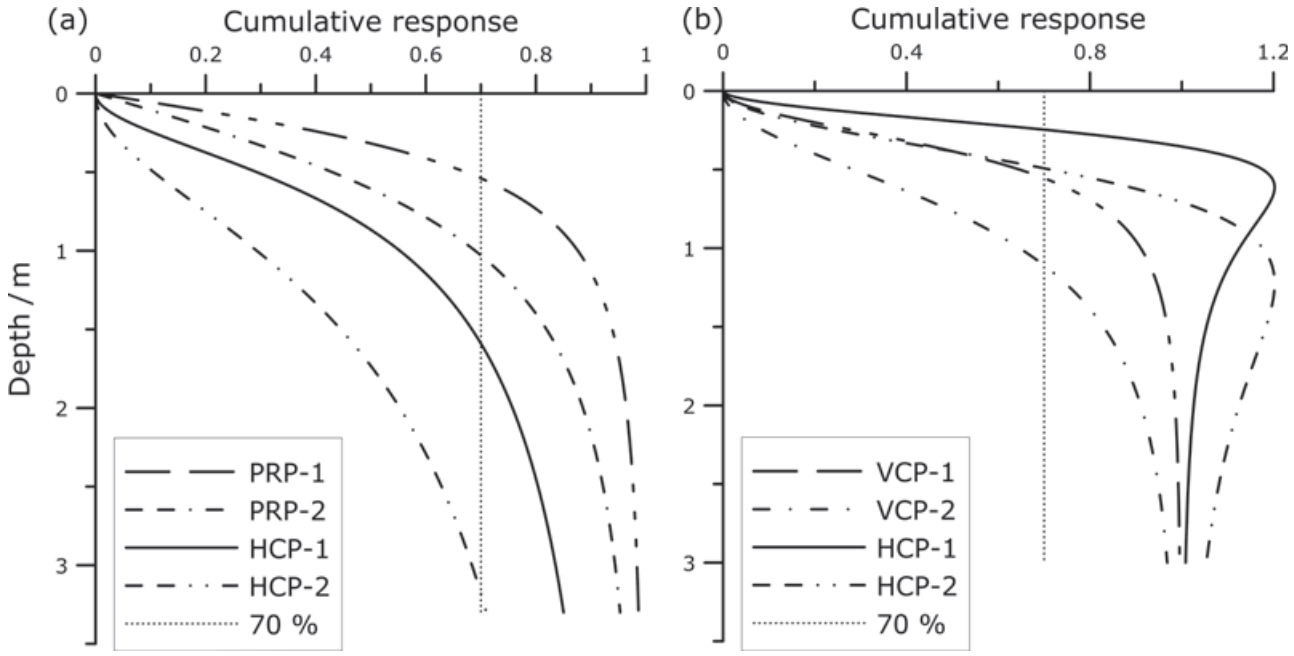


**Figure 2** Cumulative depth response curves of the apparent electrical conductivity (ECa) and apparent magnetic susceptibility (MSa) measurements for different EMI coil configurations and with indication of the 70% cumulative response (DOE).

transmitter-receiver coil spacing;

$$\begin{aligned} \mathrm{MSa}_{\mathrm{HCP},s} = &\left[R_{\mathrm{HCP},s}\,(z_1) - R_{\mathrm{HCP},s}\,(z_s)\right]\cdot \mathrm{MS}_1^* \\ &+ \left[R_{\mathrm{HCP},s}\,(z_2) - R_{\mathrm{HCP},s}\,(z_1)\right]\cdot \mathrm{MS}_2^* \\ &+ \left[1 - R_{\mathrm{HCP},s}\,(z_2)\right]\cdot \mathrm{MS}_3^*, \end{aligned} \tag{7}$$

$$\begin{aligned} \mathrm{MSa}_{\mathrm{VCP},s} = &\left[R_{\mathrm{VCP},s}\,(z_1) - R_{\mathrm{VCP},s}\,(z_s)\right]\mathrm{MS}_1^* \\ &+ \left[R_{\mathrm{VCP},s}\,(z_2) - R_{\mathrm{VCP},s}\,(z_1)\right]\mathrm{MS}_2^* \\ &+ \left[1 - R_{\mathrm{VCP},s}\,(z_2)\right]\mathrm{MS}_3^*, \end{aligned} \tag{8}$$

where $R_{\mathrm{HCP},s}(z)$ and $R_{\mathrm{VCP},s}\,(z)$ are the cumulative MSa responses above depth $z$ for the HCP and VCP modes, respectively, and $z_1$ represents the depth boundary between the first and second soil volume and $z_2$ the boundary between the second and third soil volume. At every measurement location both sets of equations (Equations (5) and (6) or (7) and (8)) can be solved using the Levenberg-Marquardt non-linear least-squares algorithm (Marquardt, 1963), which converged to a stable solution to identify the unknown EC and MS values that are either $\mathrm{EC}_1^*$, $\mathrm{EC}_2^*$ and $\mathrm{EC}_3^*$ or susceptibilities $\mathrm{MS}_1^*$, $\mathrm{MS}_2^*$ and $\mathrm{MS}_3^*$, which are the conductivity and susceptibility values from the soil volumes between 0 and $z_1$ m, between $z_1 - z_2$ m and deeper than $z_2$ m, respectively.

The major advantage of isolating the contribution to EC or MS of a particular depth-slice is that its interpretation can be linked to a particular depth interval. This interpretation is much more ambiguous when based on the ECa measurements. Despite the concept of a DOE for each particular coil configuration, there is still an influence of deeper layers or objects for which the contribution is difficult to assess. Moreover, the depth-slices integrate the measurements of the four coil configurations, facilitating the removal of measurement noise.

### *Soil sensor survey*

The study area was investigated with the DUALEM-21S EMI instrument (DUALEM, Milton, Canada), which was fixed in a non-metal sledge and pulled behind an all-terrain vehicle at a speed of about 6–10 km hour$^{-1}$, crossing the field with parallel survey lines 0.85 m apart. The height of the sensor above the soil surface ($z_s$) was 0.1 m. The two-times-four simultaneous ECa measurements (both in HCP and VCP orientations) were recorded by a field computer at a frequency of about 8 Hz. The computer was also connected to a Trimble (Trimble, Sunnyvale, California, USA) AgGPS332 receiver with an Omnistar differential correction, allowing for the geo-referencing of the data with a pass-to-pass accuracy of approximately 0.05 m. Within survey lines, measurement intervals were at about 0.2 m.

The survey took place between 18 and 22 October 2011 (2 days each in HCP or VCP orientation). During this period it did not rain and the weather was stable, with a mean daily soil temperature of 11 °C. The measurements were post-processed to remove instrumental drift, 'destriped' to reduce back-lagging of the measurements and corrected to a reference temperature of 25 °C. All ECa and MSa measurements and their derived variables were interpolated to a 0.1 m by 0.1 m grid with ordinary point kriging (Goovaerts, 1997). One of the advantages of kriging is its ability to account for the in-line clustered nature of sensor

**Table 1** Descriptive statistics ($m$, mean; Min, minimum; Max, maximum; $SD$, standard deviation) of the ECa and MSa measurements ($n = 347\,423$)

| Variable | $m$ | Min | Max | SD |
|---|---|---|---|---|
| | ECa / mS m$^{-1}$ | | | |
| PRP-1 | 11 | −9 | 32 | 4.2 |
| PRP-2 | 18 | −7 | 54 | 9.0 |
| HCP-1 | 25 | −7 | 63 | 11.0 |
| HCP-2 | 34 | −7 | 89 | 15.5 |
| | MSa / $10^{-4}$ msu SI | | | |
| HCP-1 | 13 | 12 | 28 | 2.4 |
| HCP-2 | 34 | −33 | 51 | 3.9 |
| VCP-1 | −1.8 | −13 | 11 | 2.3 |
| VCP-2 | 11 | −55 | 30 | 3.6 |

measurements. We used a maximum of 64 neighbours within a circular search area around the location being interpolated, and a (spherical or exponential) variogram model that was manually fitted for every signal individually.

## Results

### *Apparent electrical conductivity (ECa)*

Some summary statistics of the $4 \times 347\,423$ ECa measurements are given in Table 1. The standard deviations increase threefold from the shallowest PRP-1 to the deepest HCP-2 coil configuration, indicating that, on average, the soil of the area becomes more heterogeneous with increasing depth. The mean ECa also increases with increasing DOE, indicating that the subsoil is on average much more conductive than the topsoil. It is rather common to observe an increase in ECa with increasing DOE, which is generally because of an increase in soil moisture. However, in this case the increase is pronounced and is most probably also influenced by an average increase in clay content with depth (Saey *et al.*, 2009b). The small negative minimum values of the ECa measurements are rather common for arable land. These are mostly caused by artefacts, such as small pieces of metal contained in the plough layer (Saey *et al.*, 2011b).

The four ECa maps are shown in Figure 3, representing a DOE-sequence of 0.5, 1.0, 1.5 and 3.2 m (note the difference in the maximum values of the colour scales). All ECa were interpolated with ordinary point kriging, using a maximum of 64 neighbours within a circular search area around the location being interpolated. We modelled the variograms by manually fitting a model to the experimental values. For comparative reasons we standardized the variogram of every coil configuration by dividing it by the corresponding data variance (Figure 4). It will be clear that the sensor measurements result in smooth experimental variogram data with a very small nugget effect, which can be modelled in a straightforward way. The data from the PRP-1 coil configuration displayed a larger standardized semivariance at short lag distances than the other coil configurations. This reveals that the PRP-1 coil configuration, with the smallest DOI, has the largest relative variability at short distances. Moreover, the relative semivariance of this PRP-1 coil configuration was, on average, substantially larger than those of the PRP-2 coil configuration, which was, in turn, larger than the semivariance of the HCP coil configurations. This indicates that the topsoil is relatively more variable than the subsoil.

The PRP-1 (Figure 3a) map indicates that in the southern and eastern part of the study site the ECa values were small and increased towards the northwest. However, west of the amphitheatre an area of about 1 ha had a smaller conductivity and was surrounded by larger values (Figure 3a). Both to the southwest and northwest of this area of small ECa-values, small curved patterns are visible. Furthermore, several linear patterns can be seen in the northern half of the study area and a major curved structure crosses the study site from the southwest to the northeast. The other three ECa maps show similar patterns, indicating that the build-up of the soil profile in this area was homogeneous with respect to the topsoil. However, the strong and continuous increase of the larger ECa values from the PRP-1 configuration compared with the PRP-2, HCP-1 and HCP-2 configurations indicates that in zones with large ECa, the subsoil became increasingly more conductive with depth. On the other hand, the zones with small ECa in the PRP-1 configuration had a small ECa in the other three configurations. Therefore, the sub-soil of these zones did not show an increase in conductivity with depth.

### *Apparent magnetic susceptibility (MSa)*

Table 1 also provides the statistics for the four MSa measurements. These are less straightforward to interpret because they have more complex depth response curves. However, the measurements obtained with the 1-m coil spacing were, for both the HCP and VCP orientations, on average, smaller and less heterogeneous than those measured with 2-m coil spacing.

Figure 5 shows four MSa measurements obtained with the 1 and 2 m HCP and VCP orientations (observe the inverted scale between the HCP and VCP maps to account for the reversed magnetic response between these coil orientations). The HCP-1 measurements depict a continuous magnetic variation across the study area with strong contrasts between the north-eastern part and the southern and eastern parts. Both the HCP-2 and VCP-1 configurations reveal the archaeological structures from the school of gladiators. Complementary structures are visible on the VCP-2 measurements. The curved structure observed with the ECa measurements in the PRP-1 configuration, crossing the area from the southwest to the northeast, was visible on all four MSa maps, but can be best seen in the HCP-2 and the VCP-2 configurations. This structure, which is also clearly shown in the magnetic and GPR data, is thought to be one of the major water delivery canals (aqueduct) to the town of Carnuntum (its walls were situated about 0.15 km to the northeast of the study area).

### *Stratigraphy*

Given the pedology of the study area, we assumed a two-layer stratigraphic model: a gravel substrate below a loess

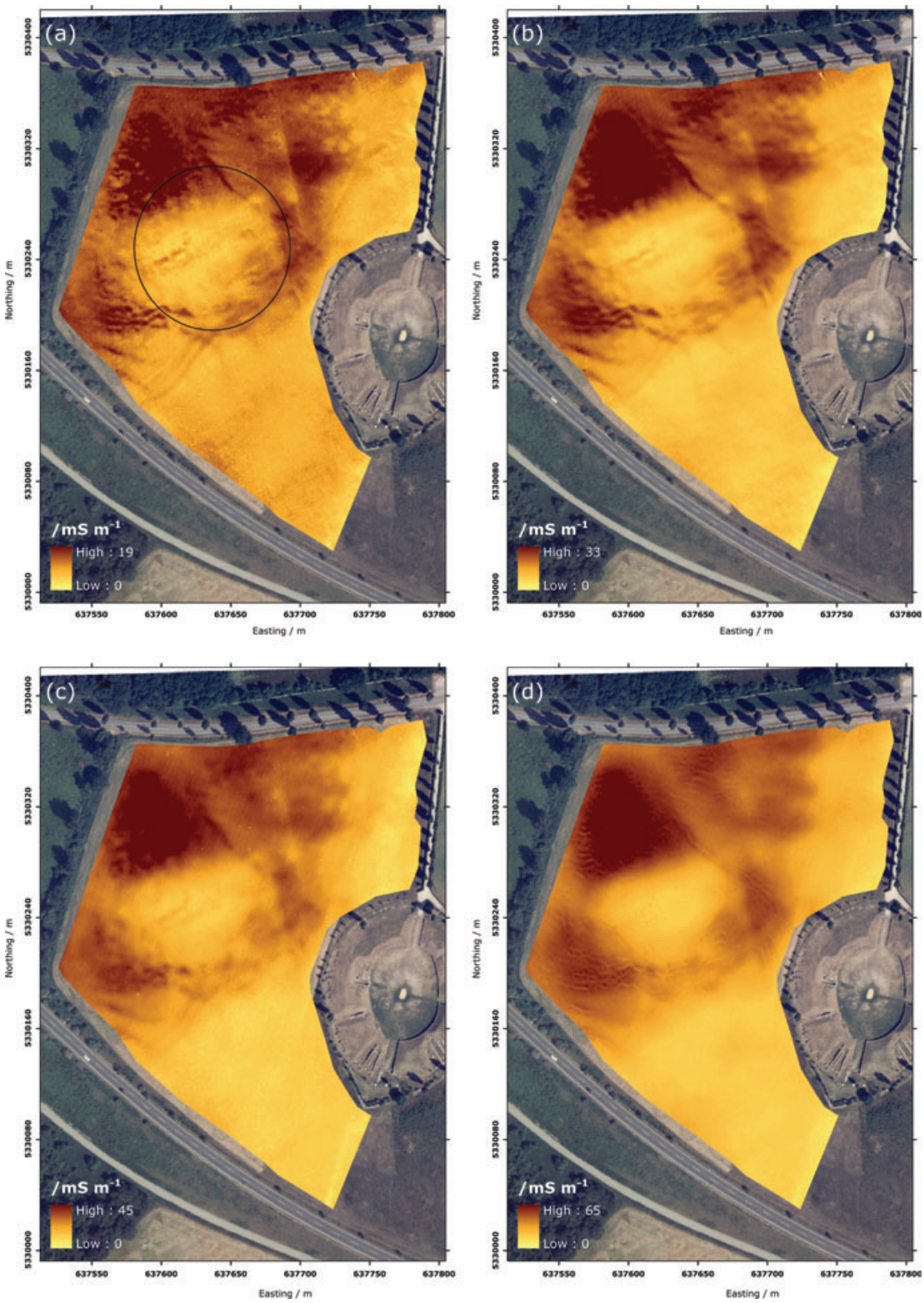


**Figure 3** Apparent electrical conductivity (mS m$^{-1}$) obtained with the four different coil configurations of the EMI sensor: (a) PRP-1, (b) PRP-2, (c) HCP-1 and (d) HCP-2, with delineation of the low-conductive region next to the amphitheatre.

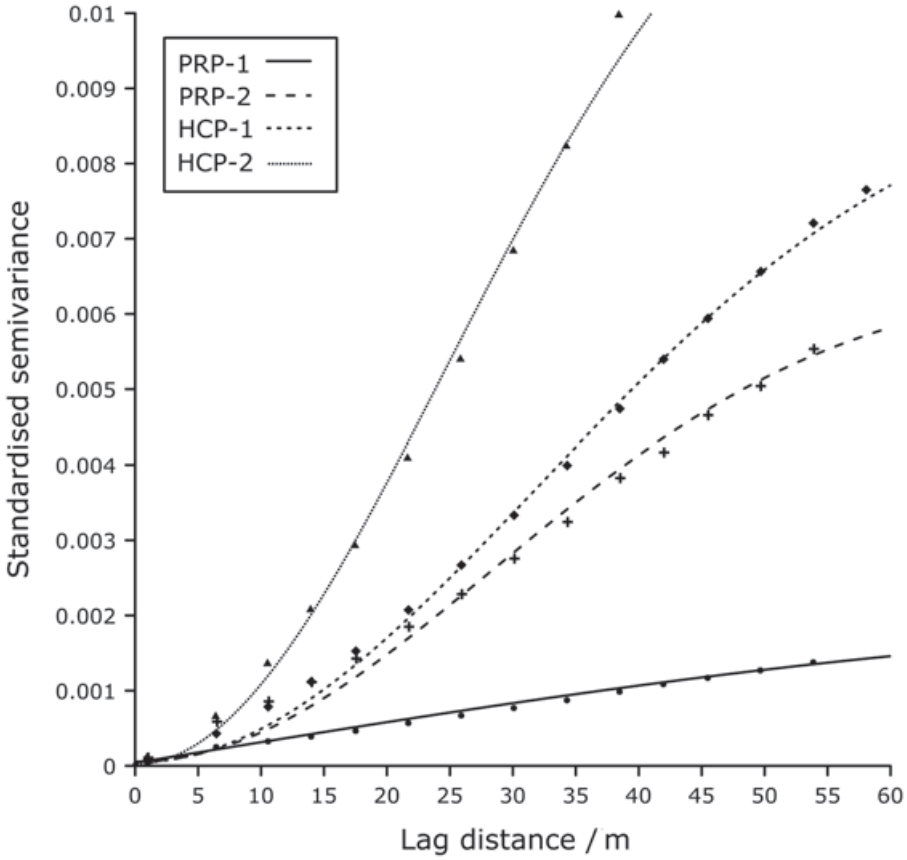


**Figure 4** Standardized variogram models of the ECa measurements.

deposit of varying thickness (Neubauer *et al.*, 2002). Given this two-layer stratigraphic model, the measured ECa of the four coil configurations can each be estimated by summing the conductivities and depth-weighted contributions of the two layers.

Because of the impossibility of obtaining soil auger observations, the conductivities of both the loess topsoil ($EC_{top}$) and gravel substrate ($EC_{sub}$) were assumed to be homogeneous across the study site. The unknown and fixed parameters $EC_{top}$ and $EC_{sub}$ will be empirically determined by fitting the ECa measurements from the HCP-1 configuration ($ECa_{HCP,1}$), modelled by employing the ECa measurements from the HCP-2 configuration ($ECa_{HCP,2}$) measurements, to the measured $ECa_{HCP,1}$.

The depth between the topsoil and the gravel ($z^*$) can be modelled from Equation (1) given the $ECa_{HCP,2}$ measurements. Therefore, $R_{HCP,2}(z^*)$ was calculated given the ECa measurements and the unknown conductivities of both layers ($EC_{top}$ and $EC_{sub}$):

$$R_{HCP,2}\left(z^*\right) = \frac{ECa_{HCP,2} + R_{HCP,2}\left(0.16\right) \cdot EC_{top} - EC_{sub}}{EC_{top} - EC_{sub}}. \quad (9)$$

This calculated $R_{HCP,2}(z^*)$ value can be entered into Equation (1) to obtain $z^*$:

$$z^* = 2 \cdot \left( \frac{1}{4 \cdot \left[1 - R_{HCP,2}\left(z^*\right)\right]^2} - 0.25 \right)^{0.5} - 0.16. \quad (10)$$

Finally, $ECa^*_{HCP,1}$ was calculated using the modelled $z^*$ as:

$$ECa^*_{HCP,1} = \left[R_{HCP,1}\left(z^*\right) - R_{HCP,1}\left(z_s\right)\right] EC_{top} + \left[1 - R_{HCP,1}\left(z^*\right)\right] EC_{sub}. \quad (11)$$

To fit the model parameters $EC_{top}$ and $EC_{sub}$, the sum of the squared differences between $ECa_{HCP,1}$ and $ECa^*_{HCP,1}$ was minimized as:

$$\sum_{i=1}^{n} \left[ECa_{HCP,1}\left(i\right) - ECa^*_{HCP,1}\left(i\right)\right]^2 = \min, \quad (12)$$

with $i$ the number of the observation and n the total amount of observations.

These values were 100 and 9 mS m$^{-1}$, respectively. Given these values, $z^*$ was non-linearly transformed from the $ECa_{HCP,2}$ by combining Equations (1) and (10) for each of the 347 423 measurement locations. Figure 6 shows the position of this interface.

### *Depth-slicing*

The four ECa and MSa measurements were transformed into three EC and three MS-depth-slices with $z_1 = 0.5$ m and $z_2 = 1$ m:

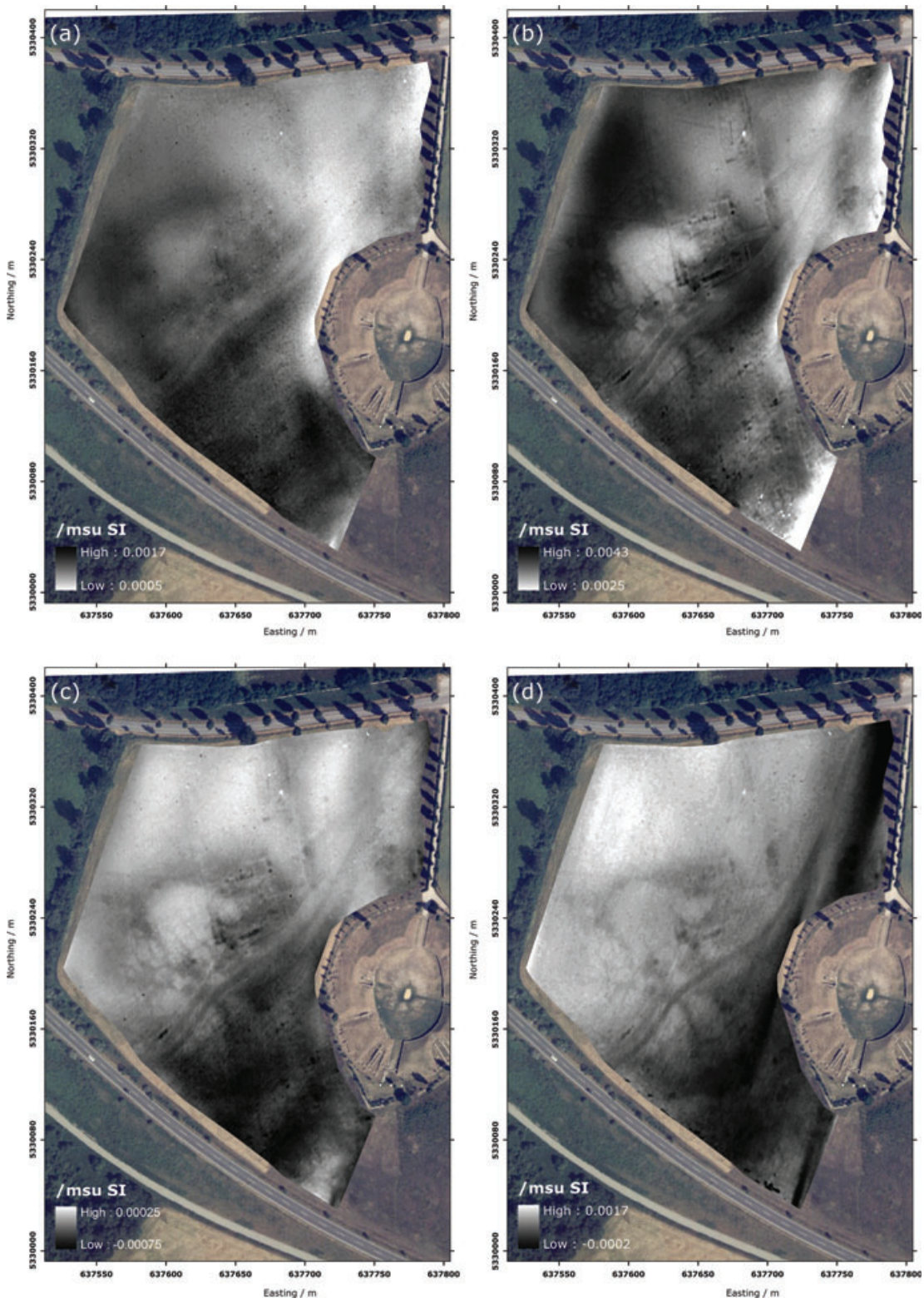


**Figure 5** Apparent magnetic susceptibility (msu SI) obtained with four different coil configurations of the EMI sensor: (a) HCP-1, (b) HCP-2, (c) VCP-1 and (d) VCP-2.

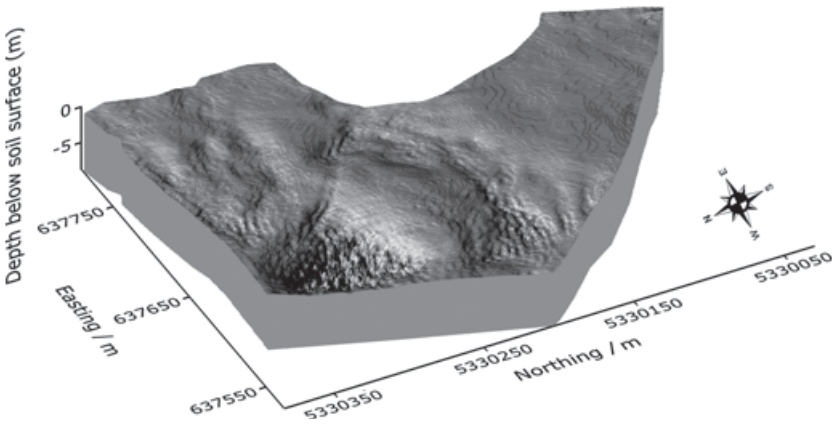


**Figure 6** Three-dimensional representation of the depth of the soil-gravel interface below the soil surface.

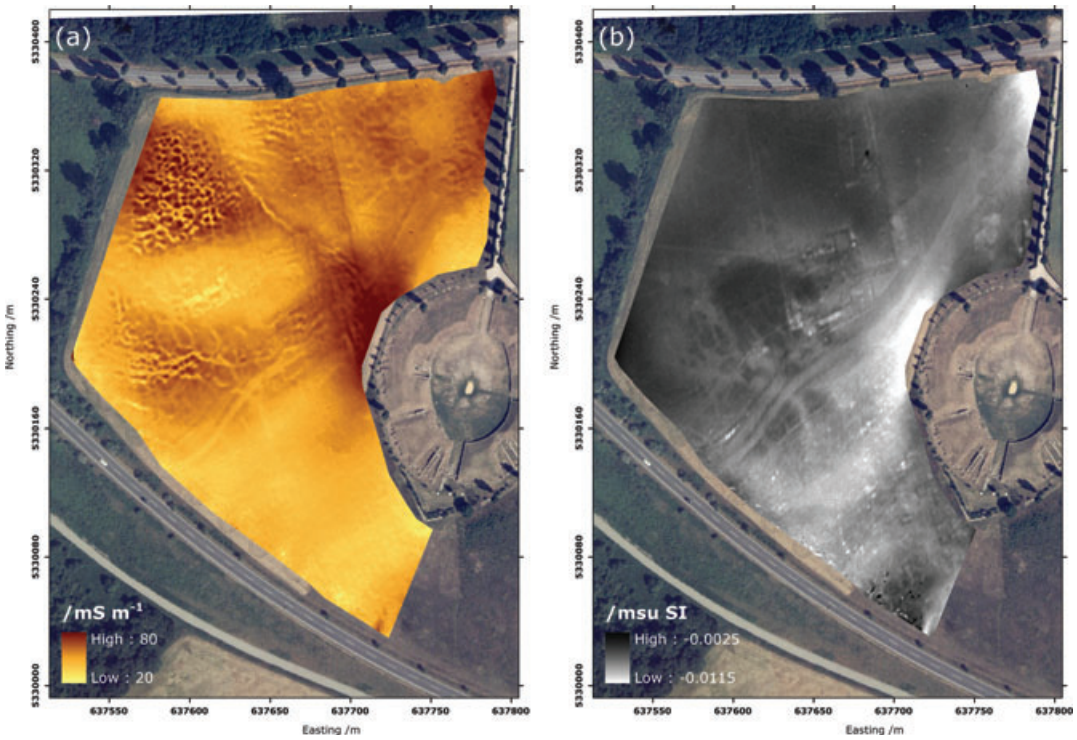


**Figure 7** (a) Electrical conductivity (mS m$^{-1}$) of the top depth slice (0–0.5 m) ($EC_1^*$); (b) magnetic susceptibility (msu SI) of the deep depth slice (> 1.0 m) ($MS_3^*$).

Equations (5), (6), (7) and (8). These depths were chosen to represent three slices termed 'top' (0–0.5 m, with $EC_1^*$ and $MS_1^*$ representing the values of this slice), 'intermediate' (0.5–1.0 m, with $EC_2^*$ and $MS_2^*$ representing the values of this slice) and 'deep' (> 1.0 m, with $EC_3^*$ and $MS_3^*$ representing the values of this slice). Therefore, we present only two of the most informative of these six layers: $EC_1^*$ and $MS_3^*$ (Figure 7).

### *Topography and flowlines*

The differential GPS recorded also the elevation of the soil surface ($Z$) with a relative point-by-point accuracy of less than 10 cm. We used these measurements to reconstruct the current topography (Figure 8a). Next, we overlaid the $EC_1^*$ values shown in Figure 7(a) on this topography (Figure 8b).

In order to evaluate the continuity of the drainage patterns and their link to the present topography the run-off over the current surface was modelled using the module RUNOFF of the Geographical Information System 'Idrisi Kilimanjaro' (Clark Labs, Worcester, MA, USA). The result is shown in Figure 8(c).

## Discussion and conclusions

By comparing Figure 3, showing the ECa measurements, with Figure 6, depicting the soil-gravel interface, it can be seen that where small ECa values were measured, the interface is situated

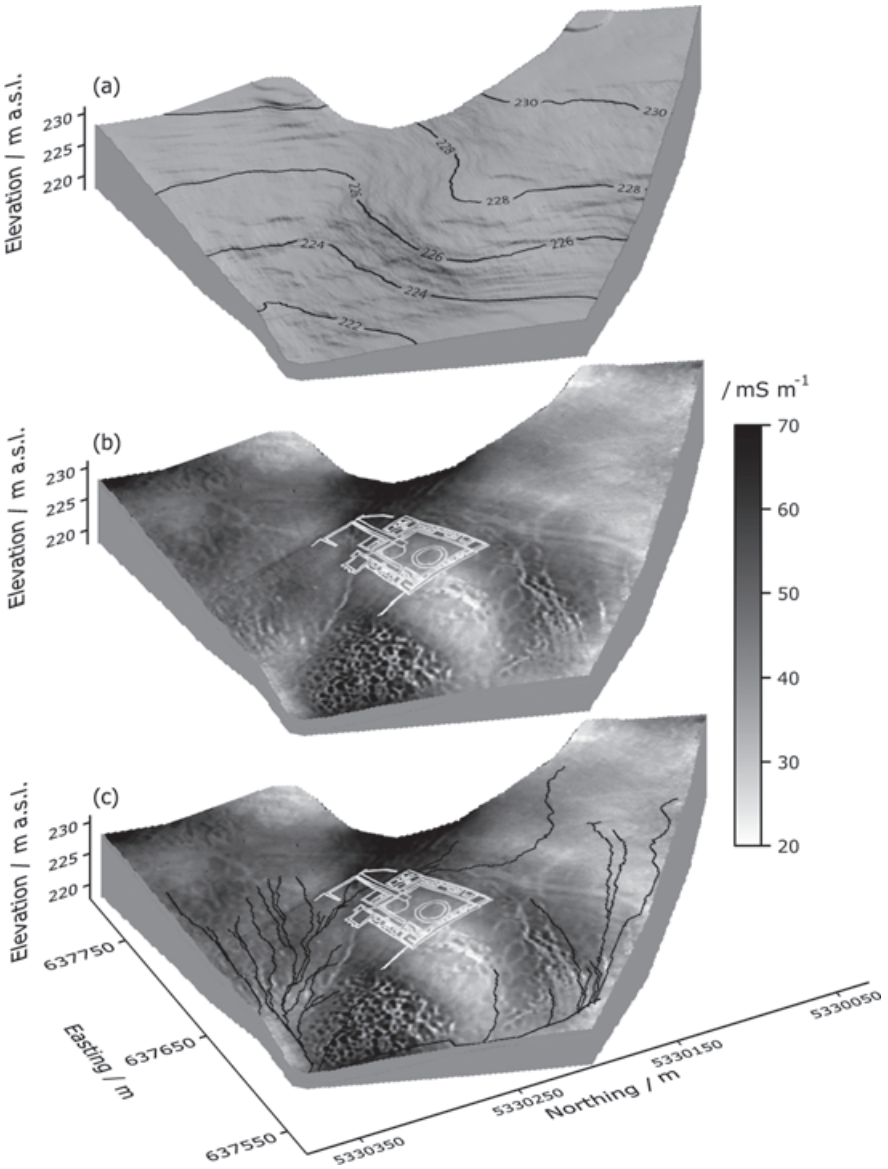


**Figure 8** (a) Current topography $Z$; (b) current topography overlain with $EC_1^*$ of the top depth slice (0–0.5 m) and outlines of the school of gladiators; (c) current topography overlain with $EC_1^*$ of the top depth slice (0–0.5 m), outlines of the school of gladiators and simulated flowlines.

near or even at the soil surface. This situation is mainly found in the southern (highest) part of the study area and in its centre. It is likely that loess might have been eroded from the higher zones of the study area and then been deposited in the lowest north-western part. The central gravel outcrop largely coincides with the location of the school of gladiators. This raises the hypothesis that the Romans used this outcrop near the amphitheatre because it provided a stable and erosion-free basis on which to build the school. As mentioned before, it was not possible to make auger observations at this protected site to verify the correctness of the proposed stratigraphic model.

The ECa measurement with the shallowest DOE (Figure 3a) indicated the presence of several small-scale features. However, as Figure 7(a) shows, the depth slicing resulted in an enhanced contrast between these features and their background. In the north-western area, where all ECa maps (Figure 3) indicated the largest values, a polygonal network appears. From previous experience with EMI sensors, we interpreted this network as frost-wedge pseudomorphs (Meerschman *et al.*, 2011). These structures are the remains of thermal contraction cracks formed in permafrost-affected soils. This means that the soil of this part of the study area remained largely unaffected since the last period of permafrost, which was during the very cold Dryas phases of the Weichselian Late-Glacial period, some 13 000 to 10 000 years BP (Lowe & Walker, 1997). In the central and north-eastern parts of the study area traces of surface drainage patterns were clearly visible. As no erosion phenomena were currently observable it can be assumed that the detected erosion gullies were no longer active. They have been filled up with contrasting material to that of the surrounding soil. Most of these gullies flow into the lower part of the area where the frost-wedge pseudomorphs are present. Therefore, it seems likely that this surface drainage process was

the driving force for the transport and deposition of the clayey material present in the lowest part of the area. As this part was not disturbed since the Weichselian Late-Glacial it seems plausible that these erosion patterns originate from warmer and wetter phases during the Weichselian Late-Glacial period (such as the Allerød or Bølling interstadials).

The modelled layer of magnetic susceptibility $MS_3^*$ (Figure 7b) best summarizes the archaeological traces related to the school of gladiators and its associated structures. The presence of these features within this depth-slice indicates that their remains extend below a depth of 1 m. The school itself consists of an entrance hall oriented to the east. It leads into a large complex with several compartments of varying dimensions and a central open area with a circular structure. The latter was identified by high-resolution GPR measurements as a training arena. To the west of the school a small curved structure extends from the back wall of the school crossing the traces of the erosion gullies. As this structure joins the major water delivery canal (aqueduct) crossing the area from the southwest to the northeast in-between the school and the amphitheatre, it is most likely the main fresh water supply of the school. North of the school, elongated linear structures indicate the presence of the remains of a wall, probably enveloping an outside training area for horses and associated activities. At the southern rim of the amphitheatre, traces of small rectangular enclosures are visible, which were interpreted as burial monuments. It seems likely that the separated cemetery was located immediately behind the *ludus*. These findings are in good agreement with the results and interpretations of the GPR survey.

The integrated representation of Figure 8 aids the interpretation of the school of gladiators in the local soil landscape. The low-lying part with the frost-wedge pseudomorphs can easily be distinguished from the central, elevated part where the school was built. The traces of the past drainage patterns flow around the elevated section into the lower parts of the study area. It can be seen from Figure 8(c) that there is great similarity between the flow-lines across the current surface and the traces of the drainage structures in the soil. This suggests that the topography of the area has not changed substantially since the Weichselian Late-Glacial period. Therefore the current topography must be similar to the landscape wherein the Romans built the school of gladiators.

To conclude, the great potential of multi-receiver EMI for soil landscape research of an archaeological site was demonstrated. Both the pedological variability and small anthropogenic and natural features were simultaneously detected by integrating the multiple signals of both the complementary electrical conductivity and magnetic susceptibility. The ECa measurements allowed the interpretation of the soil landscape by differentiating between gravel outcrops and zones covered with a substantial loess layer. In addition, small features, such as frost-wedge pseudomorphs and drainage gullies, could be identified. The buried remains of the school of gladiators and related Roman structures were distinguished from the complementary MSa data. An integrated visualization, employing a digital elevation model of the study site, allowed us to explain the school's topographic location embedded in the soil landscape. This study resolved questions about the soil landscape around the school, thus aiding its geographical interpretation.

## Acknowledgements

The authors would like to thank Valentijn Van Parys for his assistance with the fieldwork and Mr Traun for granting us access to his field.

## References

Clark, A. 1997. *Seeing Beneath the Soil. Prospecting Methods in Archaeology*. B.T. Batsford Ltd, London.

De Clercq, W., De Smedt, P., De Reu, J., Herremans, D., Masters, P., Saey, T. *et al.* 2012. Towards an integrated methodology for assessing rural settlement landscapes in the Belgian lowlands. *Archaeological Prospection*, **19,** 141–145.

Fleisch, D. 2008. *A Student's Guide to Maxwell's Equations*. Cambridge University Press, New York.

Frischknecht, F.C., Labson, V.F., Spies, B.R. & Anderson, W.L. 1991. Profiling methods using small sources. In: *Electromagnetic Methods in Applied Geophysics-Applications Part A and Part B* (ed. M.N. Nabighian), pp. 105–270. Society of Exploration Geophysicists, Tulsa, OK.

Gaffney, C. & Gater, J. 2003. *Revealing the Buried Past: Geophysics for Archaeologists*. Tempus Publishing, Stroud.

Goovaerts, P. 1997. Geostatistics for Natural Resources Evaluation, *Applied Geostatistics Series*. New York, Oxford University Press.

Heil, K. & Schmidhalter, U. 2012. Characterisation of soil texture variability using the apparent electrical conductivity at a highly variable site. *Computers & Geoscience*, **39,** 98–110.

Hendrickx, J.M.H., Borchers, B., Corwin, D.L., Lesch, S.M., Hilgendorf, A.C. & Schlue, J. 2002. Inversion of soil conductivity profiles from electromagnetic induction measurements. *Soil Science Society of America Journal*, **66,** 673–685.

Humer, F. 2012. Einblicke in das leben Römischer gladiatoren. *Acta Carnuntina*, **2,** 16–33.

IUSS Working Group WRB 2006. *World Reference Base for Soil Resources 2006*. World Soil Resources Reports No 103, FAO, Rome.

Lowe, J.J. & Walker, M.J.C. 1997. *Reconstructing Quaternary Environments*. Pearson Educational Limited, Harlow.

Lück, E. & Ruehlmann, J. 2013. Resistivity mapping with Geophilus Electricus – information about lateral and vertical soil heterogeneity. *Geoderma*, **119**, 2–11.

Marquardt, D. 1963. An algorithm for least-squares estimation of nonlinear parameters. *SIAM Journal on Applied Mathematics*, **11,** 431–441.

Maxwell, J.D. 1865. A dynamical theory of the electromagnetic field. *Philosophical Transactions of the Royal Society of London*, **155,** 459–512.

McBratney, A., Minasny, B. & Whelan, B.M. 2005. Obtaining 'useful' high-resolution soil data from proximally-sensed electrical conductivity/resistivity (PSEC/R) surveys. In: *Precision Agriculture '05* (ed. J.V. Stafford), pp. 503–510. Wageningen Academic Publishers, Wageningen.

McNeill, J.D. 1980. *Electromagnetic Terrain Conductivity Measurement at Low Induction Numbers*, Technical Note TN-6. Geonics Limited, Missisauga.

Meerschman, E., Van Meirvenne, M., De Smedt, P., Saey, T., Islam, M.M., Meeuws, F. *et al.* 2011. Imaging a polygonal network of ice-wedge casts with an electromagnetic induction. *Soil Science Society of America Journal*, **75,** 1–6.

Monteiro Santos, F.A., Triantafilis, J., Bruzgulis, K.E. & Roe, J.A.E. 2010. Inversion of multiconfiguration electromagnetic (DUALEM-421) profiling data using a one-dimensional laterally constrained algorithm. *Vadose Zone Journal*, **9,** 117–125.

Neubauer, W., Eder-Hinterleitner, A., Seren, S. & Melichar, P. 2002. Georadar in the Roman civil town Carnuntum, Austria: an approach for archaeological interpretation of GPR data. *Archaeological Prospection*, **9,** 135–156.

Neubauer, W., Doneus, M., Trinks, I., Verhoeven, G., Hinterleitner, A., Seren, S. *et al.* 2012. Long-term Integrated Archaeological Prospection at the Roman Town of Carnuntum/Austria. In: *Archaeological survey and the city* (eds. P. Johnson & M. Millett), pp. 202–221. Oxbow Books, Oxford, UK.

Saey, T., Simpson, D., Vermeersch, H., Cockx, L. & Van Meirvenne, M. 2009a. Comparing the EM38DD and DUALEM-21S sensors for depth-to-clay mapping. *Soil Science Society of America Journal*, **73,** 7–12.

Saey, T., Van Meirvenne, M., Vermeersch, H., Ameloot, N. & Cockx, L. 2009b. A pedotransfer function to evaluate the soil profile textural heterogeneity using proximally sensed apparent electrical conductivity. *Geoderma*, **150,** 389–395.

Saey, T., Van Meirvenne, M., De Smedt, P., Cockx, L., Meerschman, E., Islam, M.M. *et al.* 2011a. Mapping depth-to-clay using fitted multiple depth response curves of a proximal EMI sensor. *Geoderma*, **162,** 151–158.

Saey, T., Van Meirvenne, M., Dewilde, M., Wyffels, F., De Smedt, P., Meerschman, E. *et al.* 2011b. Combining multiple signals of an electromagnetic induction sensor to prospect land for metal objects. *Near Surface Geophysics*, **9,** 309–317.

Saey, T., De Smedt, P., Islam, M.M., Meerschman, E., Van De Vijver, E., Lehouck, A. *et al.* 2012. Depth slicing of multi-receiver EMI measurements to enhance the delineation of contrasting subsoil features. *Geoderma*, **189–190,** 514–521.

Simpson, D., Van Meirvenne, M., Saey, T., Vermeersch, H., Bourgeois, J., Lehouck, A. *et al.* 2009. Evaluating the multiple coil configurations of the EM38DD and DUALEM-21S sensors to detect archaeological anomalies. *Archaeological Prospection*, **16,** 91–102.

Thiesson, J., Dabas, M. & Flageul, S. 2009. Detection of resistive features using towed Slingram electromagnetic induction instruments. *Archaeological Prospection*, **16,** 103–109.

Thiesson, J., Rousselle, G., Simon, F.X. & Tabbagh, A. 2011. Slingram EMI prospection: are vertical orientated devices a suitable solution in archaeological and pedological prospection? *Journal of Applied Geophysics*, **75,** 731–737.

Trinks, I., Neubauer, W. & Doneus, M. 2012. Prospecting archaeological landscapes. In: *EuroMed 2012* (eds M. Ioannides, D. Fritsch, J. Leissner, R. Davies, F. Remondino & R. Caffo), pp. 21–29. Springer, Berlin, Heidelberg.

Van Dam, R.L. 2012. Landform characterization using geophysics – recent advances, applications, and emerging tools. *Geomorphology*, **137,** 57–73.

Viscarra Rossel, R., Adamchuk, V., Sudduth, K., McKenzie, N. & Lobsey, C. 2011. Chapter five – Proximal soil sensing: an effective approach for soil measurements in space and time. *Advances in Agronomy*, **113,** 237–282.

Wait, J.R. 1962. A note on the electromagnetic response of a stratified earth. *Geophysics*, **27,** 382–385.